X-ray study of the electron density distributions for hexagonal Al_5Co_2 and $Al_{10}Mn_3$

1999 J. Phys.: Condens. Matter 11 1015

(http://iopscience.iop.org/0953-8984/11/4/009)

J. Phys.: Condens. Matter **11** (1999) 1015–1026. Printed in the UK PII: S0953-8984(99)94722-7

X-ray study of the electron density distributions for hexagonal Al_5Co_2 and $Al_{10}Mn_3$

K Yamamoto, M Jono and Y Matsuo

Department of Physics, Nara Women's University, Nara 630-5806, Japan

Received 2 June 1998, in final form 14 October 1998

Abstract. The electron density distributions of Al_5Co_2 and $Al_{10}Mn_3$, which include icosahedral clusters, have been studied by a single-crystal x-ray diffraction method. The maximum-entropy method (MEM) is used to construct the electron density distribution (EDD). In the EDD maps, strongly covalent bonds between Al atoms and transition metal (TM) atoms are visible. As regards the chemical bonding, $Al_{10}Mn_3$ has an icosahedral bonding environment, whereas Al_5Co_2 does not. The number of electrons belonging to each atom and the charge transfer from Al atoms to TM atoms have been derived from the EDD maps. The negative valences were estimated to be -1.25 and -1.26 for Co atoms and -1.00 for a Mn atom. These negative valences can be understood to be the charge transfer due to the covalent bond with strongly ionic character. These results were compared with pair-potential calculations and band-structure calculations.

1. Introduction

Al-rich Al–TM alloy systems have meta-stable decagonal (Al–Mn, Al–Co, Al–Fe, Al–Pd, etc) and icosahedral (Al–Mn, Al–Cr, etc) quasicrystals, and stable decagonal (Al–Pd–Mn, Al–Ni–Co, Al–Cu–Co, etc) and icosahedral (Al–Pd–Mn, Al–Cu–Fe, etc) quasicrystals. These alloy systems also include several crystalline intermetallic compounds ($Al_{13}Co_4$ [1], τ^n-$Al_{13}Co_4$ [2], Al_3Co [2], $Al_{11}Co_4$ [3], Al_5Co_2 [4], Al_6Mn [5], Al_4Mn [6–8], $Al_{10}Mn_3$ [9], Al_3Mn [10], etc). These intermetallic compounds include pentagonal and icosahedral clusters, the same clusters as construct the decagonal and icosahedral quasicrystals. Thus, the structures and the chemical bonds of these intermetallic compounds are of great interest in studies of the structural stability of quasicrystals. A detailed discussion of the chemical bond requires an accurate experimental study of the electron density distribution (EDD). Such a discussion could be based on an x-ray diffraction experiment and an analysis by the maximum-entropy method (MEM). So far, an experimental study of the precise EDDs for these alloy systems has not been carried out. The aim of this paper is to construct the precise EDDs of these intermetallic compounds and to find the bonds constructing the icosahedral and pentagonal clusters, and, then, to interpret the structures as regards the chemical bonding. This paper is the first in a series of studies of EDDs of Al-rich Al–TM intermetallic compounds. Al_5Co_2 and $Al_{10}Mn_3$ are treated in this paper.

Al_5Co_2 and $Al_{10}Mn_3$ have the same hexagonal prototype structure ($P6_3/mmc$) [11], which is a simple structure compared with those of other Al-rich Al–TM intermetallic compounds. The structures of Al_5Co_2 and $Al_{10}Mn_3$ have been studied using the Weissenberg camera method by Newkirk *et al* [4] and Taylor [9], respectively. These structures can be related to icosahedral and decagonal quasicrystals, because of the icosahedral and pentagonal

0953-8984/99/041015+12$19.50

atomic arrangements. Indeed, an Al–Mn alloy system has icosahedral and decagonal quasicrystalline phases for the Al_4Mn composition, whereas an Al–Co alloy system has only a decagonal quasicrystalline phase for the Al_3Co composition.

In this work, careful x-ray diffraction experiments were carried out for single crystals of Al_5Co_2 and $Al_{10}Mn_3$. The precise EDD maps are estimated by analysing diffraction data sets using the MEM. The MEM is very powerful in studying EDDs, because of its visual clarity, in particular in regions of low electron density, and because of the freedom from atomic models in the calculation. Several features of the chemical bonds in Al_5Co_2 and $Al_{10}Mn_3$ are discussed on the basis of these EDD maps. The number of valence electrons for each atom is estimated and the charge transfer from Al atoms to TM atoms is discussed. These features are compared with the results obtained by certain pair-potential calculations and band-structure calculations.

2. Experimental procedure

Alloy ingots with nominal compositions of Al_5Co_2 and $Al_{10}Mn_3$ were prepared by melting a mixture of pure elements in an Ar atmosphere using an arc furnace. These ingots were crushed into powder, put into an alumina crucible, and then sealed in a quartz tube. The powder specimens were remelted at 1373 K and slowly cooled to 1073 K at a rate of 1 K min^{-1}. After being annealed at this temperature for 24 hours, the specimens were quenched in water. Needle-like single crystals with hexa-prismatic morphology were selected.

The integrated intensity measurements for Al_5Co_2 and $Al_{10}Mn_3$ were carried out using Mo Kα radiation with an automatic single-crystal four-circle diffractometer (Rigaku AFC-5). The incident x-ray beam was monochromated by a flat graphite crystal. The distance between the crystal and the receiving slit was 275 mm, and a receiving slit of 3 mm $\times$ 3 mm was used. The collections of integrated intensities were conducted in the 2θ–ω scan mode with a scan width of $0.90^\circ + 0.35^\circ \tan\theta$. The reflections with indices $(+h, \pm k, \pm l)$ were collected up to the $2\theta_{max}$ value of 80°. Three standard reflections were monitored every 100 reflections. There was no significant change in the intensity of the standard reflections. To avoid the absorption effect and the extinction effect as far as possible in the x-ray diffraction experiments, the single crystals of Al_5Co_2 and $Al_{10}Mn_3$ were shaped into small spheres of 0.100(5) mm and 0.105(5) mm diameter, respectively.

3. Structure analysis

Before the study of the EDD, a detailed structure analysis, which refines the occupation probabilities of each of the atoms, was performed by using the full-matrix least-squares program RADIEL [12]. Weak reflections with $|F^{obs}| \leqslant 3\sigma$ were excluded from the data set, where σ is the standard deviation of the observed structure amplitude due to counting statistics. The intensities of equivalent reflections were averaged. The number of independent reflections having an effective integrated intensity were 346 for Al_5Co_2 and 366 for $Al_{10}Mn_3$, respectively. Corrections for Lorentz and polarization factors were made. Absorption corrections were made by assuming spherical shapes of the specimens. The linear absorption coefficients were self-consistently determined from the atomic occupations in the least-squares refinement.

First, the structure models given by Newkirk *et al* [4] for Al_5Co_2 and Taylor [9] for $Al_{10}Mn_3$ were refined. In the refinements, the occupation probabilities were fixed to preserve the stoichiometric composition, and anisotropic temperature factors and an isotropic extinction correction defined by Zachariasen [13] were used. Al_5Co_2 and $Al_{10}Mn_3$ have the hexagonal structure ($P6_3/mmc$) with lattice parameters $a = 7.664(2)$ Å and $c = 7.605(1)$ Å,

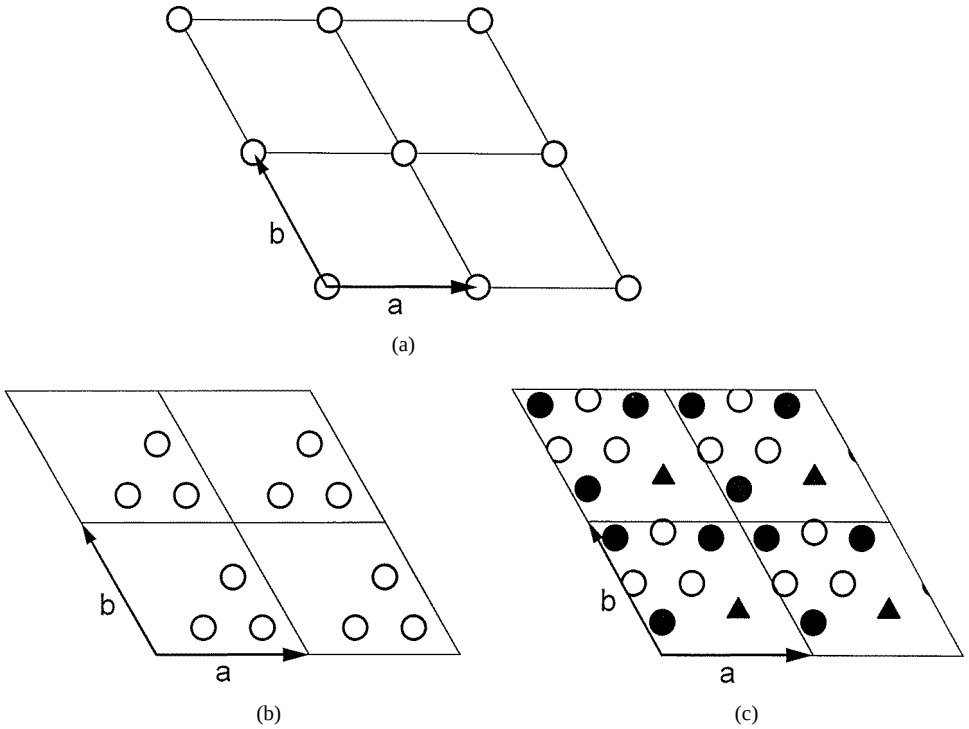

Figure 1. Atomic arrangements of successive layers for (a) layer A, (b) layer B, and (c) layer C. Open circles indicate Al atoms, where Al(1) is located in layer A, Al(3) in layer B and Al(2) in layer C. Solid circles indicate Co(1) and Mn atoms, and solid triangles indicate Co(2) and trigonal prismatic voids for Al_5Co_2 and $Al_{10}Mn_3$, respectively.

and $a = 7.546(3)$ Å and $c = 7.895(2)$ Å, and include 28 atoms and 26 atoms in a unit cell, respectively. These structure models can be divided into eight successive layers (ABCBAB′C′B′) perpendicular to the c-axis, where the layer A has the inversion centre and the layers C and C′ are located on the mirror plane. Atomic arrangements on the layers A with $z = 0$, B with $z \approx 0.06$, and C with $z = 0.25$ are shown in figures 1(a), 1(b), and 1(c), respectively. And these structures include TM-atom-centred Al icosahedra interpenetrating and connecting with each other and trigonal prismatic voids as shown in figure 2. For Al_5Co_2, Co atoms occupy these voids. These stoichiometric models show the adequately small R-factors and R_w-factors: 0.0186 and 0.0219 for Al_5Co_2 and 0.0255 and 0.0375 for $Al_{10}Mn_3$. These factors are defined by

$$R = \sum ||F^{obs}| - |F^{cal}|| \Big/ \sum |F^{obs}|$$

and

$$R_w = \left[\sum w(|F^{obs}| - |F^{cal}|)^2 \Big/ \sum w|F^{obs}|^2 \right]^{1/2}$$

where $w = 1/\sigma^2$. However, the systematic difference between observed and calculated structure factors was particularly strong for $Al_{10}Mn_3$. We tested several models introducing partial occupancies and mixing of Al and TM atoms, and the most reliable models were found to show some defects on Co(2) and Al(2) for Al_5Co_2, and on Mn, Al(2), and Al(3) for $Al_{10}Mn_3$. The values of the R-factor and R_w-factor are 0.0128 and 0.0138 for Al_5Co_2, and 0.0211 and

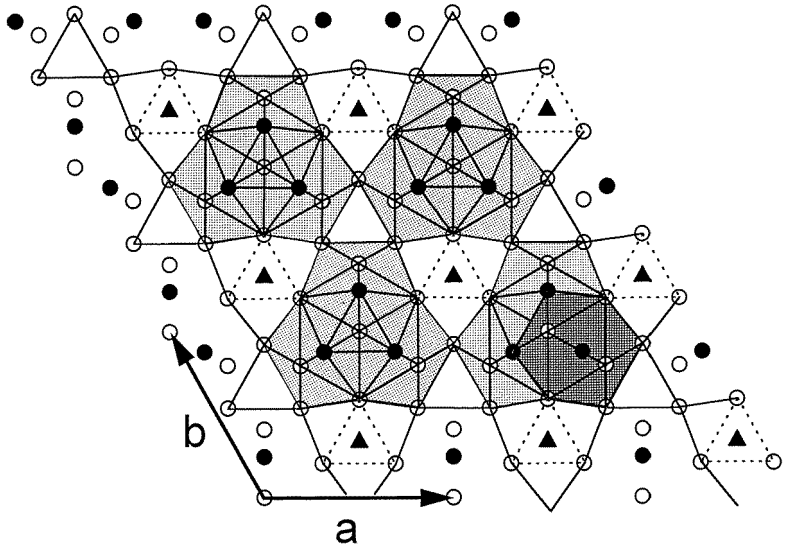

Figure 2. A partial projection of the structure model perpendicular to the c-axis. One cluster layer is shown, which is constructed from TM-atom-centred Al icosahedra interpenetrating and connecting with each other. Open circles indicate Al atoms. Solid circles and solid triangles indicate Co(1) and Mn atoms, and Co(2) atoms and trigonal prismatic voids for Al_5Co_2 and $Al_{10}Mn_3$, respectively. The deeper-grey area shows TM-atom-centred Al icosahedra, where two Al atoms change to TM atoms due to the interpenetration. The lighter-grey area shows an interpenetrated cluster with three icosahedra. The dashed lines show trigonal prisms.

Table 1. The occupation probability P, positional parameters (XYZ), thermal parameters U_{ij} ($\times 10^{-5}$), the isotropic extinction parameter g_{iso} ($\times 10^{-3}$), the refined composition, and the linear absorption coefficient (cm^{-1}) of Al_5Co_2. The form of the thermal parameter is $\exp[-2\pi^2(U_{11}h^2a^{*2} + \cdots + 2U_{12}hka^*b^* \cos\gamma + \cdots)]$.

	Al(1)	Al(2)	Al(3)	Co(1)	Co(2)
P	1	0.980(2)	1	1	0.946(2)
X	0	0.467 60(5)	0.195 19(4)	0.126 83(3)	2/3
Y	0	$2X$	$2X$	$2X$	1/3
Z	0	1/4	0.940 44(6)	1/4	1/4
U_{11}	U_{22}	80(2)	87(2)	65(1)	U_{22}
U_{22}	68(4)	100(3)	93(2)	51(1)	55(3)
U_{33}	79(5)	109(3)	87(2)	51(1)	52(3)
U_{12}	$U_{22}/2$	$U_{22}/2$	$U_{22}/2$	$U_{22}/2$	$U_{22}/2$
U_{13}	0	0	$U_{23}/2$	0	0
U_{23}	0	0	16(2)	0	0
g_{iso}	35(1)				
$Al_{19.88}Co_{7.98}$					
μ	97.67				

0.0274 for $Al_{10}Mn_3$, respectively. The results of the structure refinement are summarized in table 1 for Al_5Co_2 and in table 2 for $Al_{10}Mn_3$. Also, inter-atomic distances calculated from these results are listed in table 3.

Table 2. The occupation probability P, positional parameters (XYZ), thermal parameters U_{ij} ($\times 10^{-5}$), the isotropic extinction parameter g_{iso} ($\times 10^{-3}$), the refined composition and the linear absorption coefficient (cm^{-1}) of $Al_{10}Mn_3$. The form of the thermal parameter is $\exp[-2\pi^2(U_{11}h^2a^{*2} + \cdots + 2U_{12}hka^*b^* \cos\gamma + \cdots)]$.

	Al(1)	Al(2)	Al(3)	Mn
P	0.929(6)	0.921(4)	1	0.900(2)
X	0	0.461 36(5)	0.204 68(4)	0.122 93(3)
Y	0	$2X$	$2X$	$2X$
Z	0	1/4	0.936 29(6)	1/4
U_{11}	U_{22}	95(3)	103(2)	97(1)
U_{22}	101(6)	196(4)	109(2)	97(2)
U_{33}	417(5)	212(3)	88(2)	59(1)
U_{12}	$U_{22}/2$	$U_{22}/2$	$U_{22}/2$	$U_{22}/2$
U_{13}	0	0	$U_{23}/2$	0
U_{23}	0	0	2(1)	0
g_{iso}	95(7)			
$Al_{19.38}Mn_{5.40}$				
μ	56.14			

Table 3. Inter-atomic distances (Å) for Al_5Co_2 and $Al_{10}Mn_3$. TM stands for Co or Mn atoms.

	Al_5Co_2	$Al_{10}Mn_3$
Al(1)–Al(1)	3.797	3.940
Al(1)–Al(3)	2.628	2.721
Al(2)–Al(2)	3.084	2.894
Al(2)–Al(3)	2.753	2.771
	2.965	2.992
Al(3)–Al(3)	2.892	2.857
	2.742	2.991
	3.173	2.943
Al(1)–TM(1)	2.536	2.545
Al(2)–TM(1)	2.407	2.399
Al(2)–TM(2)	2.640	—
Al(3)–TM(1)	2.519	2.698
	2.696	2.757
Al(3)–TM(2)	2.334	—
TM(1)–TM(1)	2.913	2.782
TM(1)–TM(2)	3.864	—

4. The MEM calculation and MEM maps

In order to analyse the integrated intensities with the use of the MEM, an absolute scale of the data set and the phases of each structure factor were derived from the results of the structure refinement. Several authors have already described some kinds of MEM suitable for electron density refinement (see, e.g., [14–19]). We use the program produced by Yamamoto *et al* [19], which follows the procedure used by Sakata and Sato [18] and introduces the weighting function used by de Vries *et al* [20]. In the MEM calculations, the unit cell was divided into $90 \times 90 \times 90$ pixels, and the number of electrons in the unit cell was fixed at 471.52 for Al_5Co_2 and 386.98 for $Al_{10}Mn_3$. From trying several different weighting schemes and estimating the appropriateness of each case [19], it turned out that the most favourable weight functions are $W = ((\sin\theta)/\lambda)^{-2}$

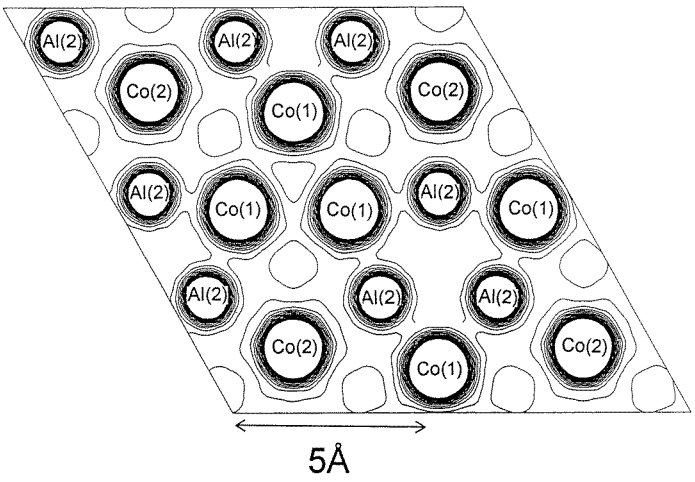

(a)

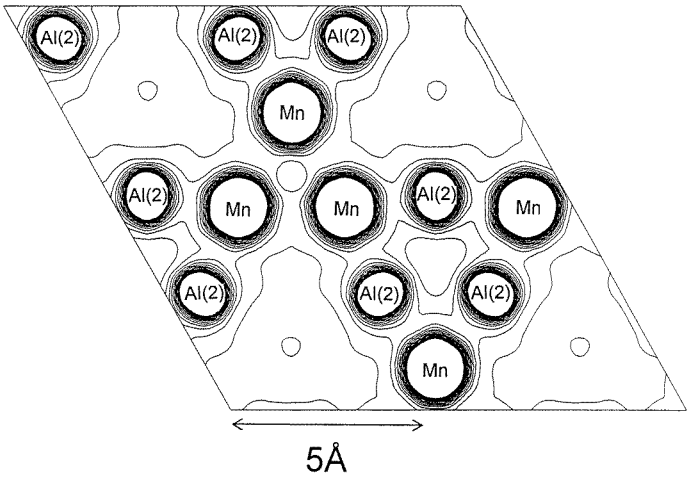

(b)

Figure 3. The EDD maps, calculated with the MEM, are perpendicular to the *c*-axis and sectioned at $Z = 1/4$ (a) for Al_5Co_2 and (b) for $Al_{10}Mn_3$, and are perpendicular to the *a*-axis and sectioned at $X = 0$ (c) for Al_5Co_2 and (d) for $Al_{10}Mn_3$. The contour lines are drawn from 0.1 to 2.0 with intervals of 0.1 (in units of electrons $Å^{-3}$).

for the Al_5Co_2 data set and $W = ((\sin\theta)/\lambda)^{-3}$ for the $Al_{10}Mn_3$ data set. The *R*-factors of the MEM refinements are 0.0142 for Al_5Co_2 and 0.0182 for $Al_{10}Mn_3$. The resolution of the MEM maps is estimated to be 0.33 Å using $r = 0.6\lambda/(2\sin\theta_{max})$.

The EDD maps calculated with the MEM are displayed in figures 3(a) and 3(c) for Al_5Co_2 and in figures 3(b) and 3(d) for $Al_{10}Mn_3$. Figures 3(a) and 3(b) are cross-sectional views of the EDDs at $Z = 1/4$ perpendicular to the *c*-axis of a hexagonal cell. The minimum heights of the electron density between the atoms are 0.29 electrons $Å^{-3}$, 0.20 electrons $Å^{-3}$, and 0.15 electrons $Å^{-3}$ for Co(1)–Al(2), Co(2)–Al(2), and Co(1)–Co(1), respectively, in figure 3(a), and 0.25 electrons $Å^{-3}$ and 0.15 electrons $Å^{-3}$ for Mn–Al(2) and Mn–Mn, respectively, in figure 3(b). Figures 3(c) and 3(d) are cross-sectional views of the EDDs at $X = 0$ perpendicular

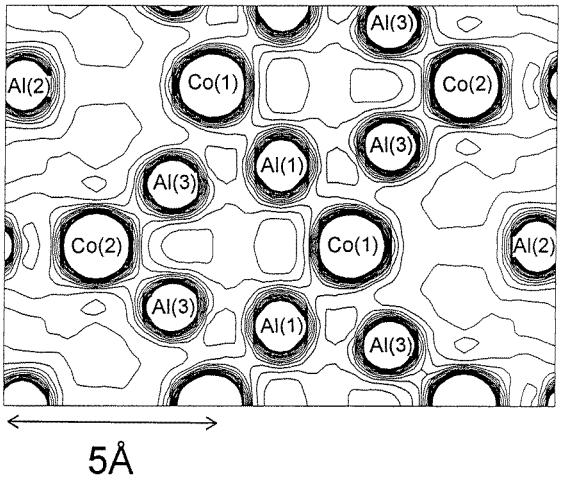

(c)

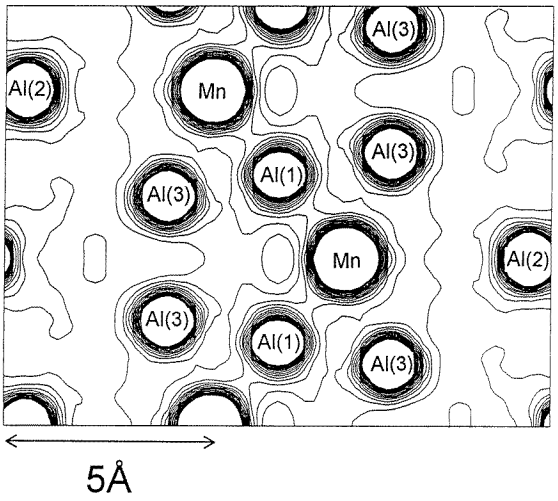

(d)

Figure 3. (Continued)

to the pseudo-fivefold *b*-axis of a hexagonal cell. The minimum heights of the electron density between the atoms are 0.33 electrons $Å^{-3}$, 0.23 electrons $Å^{-3}$, 0.42 electrons $Å^{-3}$, and 0.19 electrons $Å^{-3}$ for Co(1)–Al(1), Co(1)–Al(3), Co(2)–Al(3), and Al(1)–Al(3), respectively, in figure 3(c), and 0.31 electrons $Å^{-3}$, 0.20 electrons $Å^{-3}$, and 0.14 electrons $Å^{-3}$ for Mn–Al(1), Mn–Al(3), and Al(1)–Al(3), respectively, in figure 3(d). From the minimum heights of the electron density between the atoms and the inter-atomic distances shown in table 3, Co(1)–Al(1), Co(1)–Al(2), Co(1)–Al(3), Co(2)–Al(2), and Co(2)–Al(3) bonds for Al_5Co_2, and Mn–Al(1), Mn–Al(2), and Mn–Al(3) bonds for $Al_{10}Mn_3$ are estimated to be the direct bonds. However, the bonds between Al atoms and between TM atoms cannot be estimated to be the direct bonds, because the Co(1)- and Mn-centred icosahedra are nearly filled with electrons, and the inter-atomic distances between Al atoms are large. Therefore, it is found that the structures of Al_5Co_2 and $Al_{10}Mn_3$ are dominantly constructed from direct bonds between

Al and TM atoms. Moreover, it is found that there is a hybridization bond in Co(1)- and Mn-centred icosahedral clusters. For $Al_{10}Mn_3$, because the three kinds of Mn–Al bond have similar strengths as shown in the EDD maps, a Mn-centred icosahedron has an icosahedral bonding environment. On the other hand, for Al_5Co_2, because the Co(2)–Al(3) bond is stronger than other Al–Co bonds and the inter-atomic distance between Co(2) and Al(3) is the shortest, the icosahedral bonding environment of a Co-centred icosahedron is destroyed.

Table 4. The occupation probability P, the number of integrated electrons N_I, the number of electrons of a neutral atom N_C, and the value of the ionicity I for Al_5Co_2 and $Al_{10}Mn_3$. N_C and I are defined by $N_C = ZP$ and $I = N_C - N_I$, where Z is the atomic number.

	P	N_I	N_C	I
Al_5Co_2				
Al(1)	1.000	12.44	13.00	0.56
Al(2)	0.980	12.55	12.74	0.19
Al(3)	1.000	12.35	13.00	0.65
Co(1)	1.000	28.25	27.00	−1.25
Co(2)	0.946	26.80	25.54	−1.26
$Al_{10}Mn_3$				
Al(1)	0.929	12.16	12.08	−0.08
Al(2)	0.921	11.87	11.97	0.10
Al(3)	1.000	12.53	13.00	0.47
Mn	0.900	23.50	22.50	−1.00

The number of electrons belonging to each atom can be estimated quantitatively by integration of the EDD in an appropriate region. The integrated region should not be a spherical one having the conventional ionic or atomic radius, because these spheres cannot be embedded into the unit cell without there being unoccupied spaces. Here, an integrated region is defined as a polyhedron enclosed by boundary planes, which are possessed in common with a neighbour atom. Such a boundary plane is positioned at a point where the electron density is smallest along a direction towards a neighbour atom and is perpendicular to this direction. The unit cell is filled with the polyhedra so defined. Such polyhedra are different from the Voronoi polyhedron, because the boundary plane of the Voronoi polyhedron is at the mid-point between neighbour atoms. The results of the integration of the EDDs are summarized in table 4. For both materials, TM atoms show negative valences and Al atoms show positive valences. The valences of the Co atoms are estimated to be -1.25 and -1.26 for Co(1) and Co(2), respectively, and the valence of a Mn atom is estimated to be -1.00. These valences indicate the charge transfer from Al atoms to TM atoms.

5. Charge-transfer maps

In order to explain the charge transfer visually in detail, difference Fourier maps (charge-transfer maps) are synthesized by Fourier summation of $F^{mem}(\vec{h}) - F^{\mathrm{n-atom}}(\vec{h})$, where $F^{mem}(\vec{h})$ is the structure factor calculated from the EDDs obtained using the MEM, and $F^{\mathrm{n-atom}}(\vec{h})$ is the model structure factor constructed from neutral atoms in the structure refinement. It is worth pointing out here that the difference Fourier map defined here is different from the conventional difference Fourier map, which is defined as the Fourier summation of $F^{obs}(\vec{h}) - F^{\mathrm{n-atom}}(\vec{h})$ instead of $F^{mem}(\vec{h}) - F^{\mathrm{n-atom}}(\vec{h})$. Random errors are usually included in $F^{obs}(\vec{h})$, but are in principle excluded from $F^{mem}(\vec{h})$. The charge-transfer maps must be free from such random errors. The charge-transfer maps of the (100) plane at $Z = 1/4$ are shown in figures 4(a)

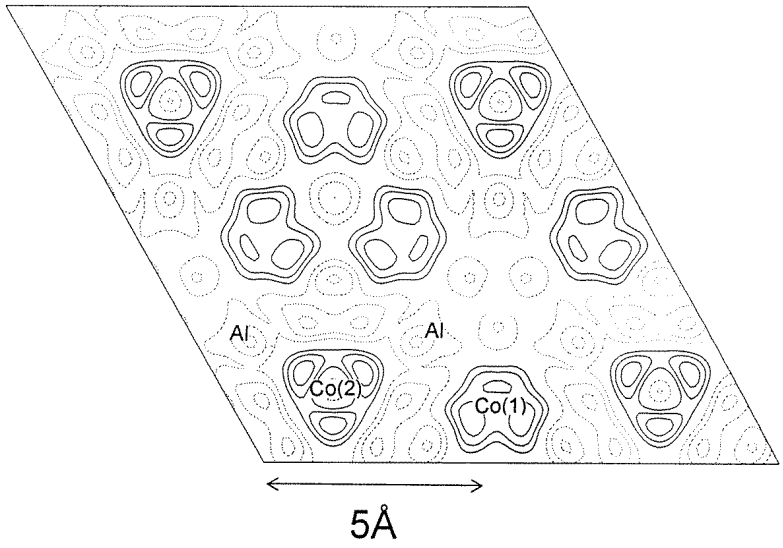

(a)

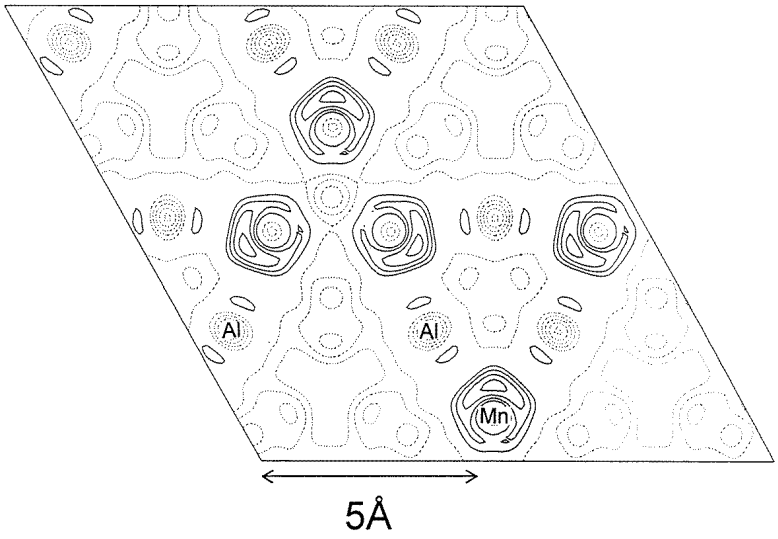

(b)

Figure 4. The charge-transfer maps, constructed by Fourier synthesizing $F^{mem}(\vec{h}) - F^{\mathrm{n-atom}}(\vec{h})$, are perpendicular to the c-axis and sectioned at $Z = 1/4$ (a) for Al_5Co_2 and (b) for $Al_{10}Mn_3$. The contour lines are drawn from -1.0 to 1.0 with intervals of 0.05 (in units of electrons $Å^{-3}$). Solid contour lines show the negative valence, and dotted contour lines show the positive valence.

and 4(b) for Al_5Co_2 and $Al_{10}Mn_3$, respectively. Solid contour lines show the negative-charge-difference density, and dotted contour lines show the positive-charge-difference density. In these figures, Co atoms and a Mn atom are located in the area with the large negative-charge-difference density, whereas Al atoms are located in the area with the positive-charge-difference density. Therefore, the charge transfers from Al atoms to TM atoms are clearly visible in the charge-transfer maps.

6. Discussion

In the analysis of the EDD, we found that a Mn atom in $Al_{10}Mn_3$ has an icosahedral bonding environment, whereas a Co(1) atom in Al_5Co_2 does not have an icosahedral bonding environment due to the existence of a Co(2) atom. Therefore, icosahedral character is not expected in the structure of Al_5Co_2. This agrees with the finding that an Al–Mn alloy system has icosahedral and decagonal quasicrystalline phases whereas an Al–Co alloy system has only a decagonal quasicrystalline phase, although Al_5Co_2 and $Al_{10}Mn_3$ can be related to icosahedral and decagonal quasicrystals.

The pair-potential calculation has been applied to a variety of structures for the Al–Co system by Phillips *et al* [21] and Öğüt and Rabe [22], and for the Al–Mn system by Mihalkovič *et al* [23]. In these studies, it was shown that the structures of Al-rich Al–TM intermetallic compounds prefer inter-atomic distances with the pair-potential minimum, and have the lowest pair-potential energy. In this paper, for Al_5Co_2, the Al–Co distances are coincident with the Al–Co pair-potential minimum, whereas the Co(1)–Co(1) distance of 2.91 Å and the Co(1)–Co(2) distance of 3.86 Å have a large disadvantage compared with the favourable distance ranges of 2.3 Å–2.8 Å and 4.0 Å–5.0 Å for the Co–Co pair potential. Therefore, Al_5Co_2 cannot have the lowest pair-potential energy. These Al–Co and Co–Co pair potentials, neglecting the d–d hybridization, are given by Phillips *et al* [21]. Moreover, Öğüt and Rabe [22] showed that the total pair-potential energy of Al_5Co_2 is significantly higher as compared with the results for Al_9Co_2 and $Al_{13}Co_4$. And they discussed the fact that the most probable reason for this overestimate of the structural energy of Al_5Co_2 is that the neglected interactions between the d shells might be starting to play an important role in its structural energies. In figure 4(a), the negative valence area belonging to a Co(1) atom has two peaks in the directions toward neighbouring Co(1) atoms. Therefore, we infer that these two peaks are a feature caused by the d–d bonds among Co(1) atoms and that these d–d bonds affect the Co–Co distances. On the other hand, for $Al_{10}Mn_3$, the Al–Mn distances are coincident with the Al–Mn pair-potential minimum; moreover, the Mn–Mn distance of 2.78 Å is also coincident with the Mn–Mn pair-potential minimum. These Al–Mn and Mn–Mn pair potentials, neglecting the d–d hybridization, are given by Mihalkovič *et al* [23]. The difference in pair-potential stability between the Co–Co distance in Al_5Co_2 and the Mn–Mn distance in $Al_{10}Mn_3$ seemed to be attributable to the following features. Because the specific feature caused by the d–d bond is not visible among Mn atoms in figure 4(b), the d–d hybridization effect among Mn atoms in $Al_{10}Mn_3$ is weaker than that among Co atoms in Al_5Co_2 or the vacancy of 10% at the Mn site weakens the d–d hybridization effect.

For Hume-Rothery alloys with TM atoms, Raynor [24] assumed that the charge transfer takes place from the sp conduction band to the d band, and the Co and Mn atoms were assigned negative valences of -1.71 and -3.66, respectively. However, in many recent band-structure calculations carried out using the linear muffin-tin orbital method in an atomic sphere approximation (LMTO-ASA) [25–29], a small charge transfer—for example, less than 0.3 of an electron per atomic sphere [26]—and a small overlap between the two spheres are assumed. In order to overcome the discrepancy between the two kinds of charge transfer, the apparent negative valence in the LMTO calculation was explained using the strong effect of the sp–d hybridization on the sp band by Mayou *et al* [27] and Trambly de Laissardière *et al* [25]. Because the sp–d hybridization increases the stability by widening the pseudogap at E_F and enhancing the magnitude of the DOS below E_F, the effective negative valence was defined as the difference between the total number of sp electrons calculated with and without sp–d hybridization to the same Fermi level [25, 27]. In these LMTO calculations, the effective negative valences of the TM atoms are about -2.5 for $Al_{12}Mn$ and -2.0 for Al_6Mn, and -1.8

for Al_9Co_2 and -0.9 for Al_5Co_2, where these values are estimated from the figure given by Mayou *et al* [27]. Here, because the sp electrons of TM atoms give a positive contribution to their valence [27], the negative valence of the Mn atoms for $Al_{10}Mn_3$ should be considerably less than the value -2.0 for Al_6Mn. In this paper, the negative valences of TM atoms obtained from the analysis of the EDDs are -1.25, -1.26, and -1.00 for Co(1), Co(2), and Mn, respectively. Therefore, the chemical valences of the Co and Mn atoms obtained from the EDDs are in good agreement with the band-theoretical valences obtained using the LMTO method. Recently, Belin-Ferré *et al* [29] discussed in detail the total and partial densities of states of Al_5Co_2 using LMTO calculations and soft-x-ray spectroscopy measurements. They pointed out that the Al 3p- and Al 3d-like states with localized or somewhat localized character overlap in energy with localized Co 3d states, and that the Al s states are of very low intensity over this energy range. From these features of the density of states and the negative valences obtained from the analysis of the EDDs, we infer that the Al–Co bonds appearing in the EDD maps of Al_5Co_2 are localized covalent ones with strongly ionic character. Therefore, we emphasize that the covalent bond with the strongly ionic character observed in the EDD maps and the sp–d hybridization required in the band-structure calculation are related to each other for Al-rich Al–TM intermetallic compounds.

We can show that the analysis of the EDDs is much more meaningful for the investigation of Al-rich Al–TM intermetallic compounds related to quasicrystals. In order to obtain a systematic understanding of some of the results indicated in this paper, analysis of the EDDs for $Al_{12}Mn$, Al_6Mn, $Al_{13}Fe_4$, Al_9Co, etc, will shortly be carried out in a series of studies of Al-rich Al–TM intermetallic compounds.

Acknowledgment

We wish to express our thanks to Dr Y Ishii, Department of Material Science, Himeji Institute of Technology, for useful discussions.

References

[1] Hudd R C and Taylor W H 1962 *Acta Crystallogr.* **15** 441
[2] Ma X L and Kuo K H 1992 *Metall. Trans.* A **23** 1121
[3] Li X Z, Shi N C, Ma X L and Kuo K H 1995 *Phil. Mag. Lett.* **72** 79
[4] Newkirk J B, Black P J and Damjanovic A 1961 *Acta Crystallogr.* **14** 532
[5] Nicol A D I 1953 *Acta Crystallogr.* **6** 285
[6] Franzen H F and Kreiner G 1993 *J. Alloys Compounds* **202** L21
[7] Shoemaker C B, Keszler D A and Shoemaker D P 1989 *Acta Crystallogr.* B **45** 13
[8] Shoemaker C B 1993 *Phil. Mag.* B **67** 869
[9] Taylor M A 1959 *Acta Crystallogr.* **12** 393
[10] Hiraga K, Kaneko M, Matsuo Y and Hashimoto S 1993 *Phil. Mag.* B **67** 193
[11] Kreiner G and Franzen H F 1995 *J. Alloys Compounds* **221** 15
[12] Coppens P, Guru Row T N, Leung P, Stevens E D, Becker P J and Yang Y W 1979 *Acta Crystallogr.* A **35** 63
[13] Zachariasen W H 1967 *Acta Crystallogr.* **23** 558
[14] Wilkins S W 1983 *Acta Crystallogr.* A **39** 892
[15] Bricogne G 1984 *Acta Crystallogr.* A **40** 410
[16] Livesey A L and Skilling J 1985 *Acta Crystallogr.* A **41** 113
[17] Navaza J 1986 *Acta Crystallogr.* A **42** 212
[18] Sakata M and Sato M 1990 *Acta Crystallogr.* A **46** 263
[19] Yamamoto K, Takahashi Y, Ohshima K, Okamura F P and Yukino K 1996 *Acta Crystallogr.* A **52** 606
[20] de Vries R Y, Briels W J and Feil D 1994 *Acta Crystallogr.* A **50** 383
[21] Phillips R, Zou J, Carlsson A E and Widom M 1994 *Phys. Rev.* B **49** 9322
[22] Öğüt S and Rabe K M 1994 *Phys. Rev.* B **50** 2075

[23] Mihalkovič M, Zhu W-J, Henley C L and Phillips R 1996 *Phys. Rev.* B **53** 9021
[24] Raynor G V 1949 *Prog. Met. Phys.* **1** 1
[25] Trambly de Laissardière G, Nguyen Manh D, Magaud L, Julien J P, Cyrot-Lackmann F and Mayou D 1995 *Phys. Rev.* B **52** 7920
[26] Fujiwara T 1989 *Phys. Rev.* B **40** 942
[27] Mayou D, Cyrot-Lackmann F, Trambly de Laissardière G and Klein T 1993 *J. Non-Cryst. Solids* **153+154** 412
[28] Trambly de Laissardière G and Fujiwara T 1994 *Phys. Rev.* B **50** 9843
[29] Belin-Ferré E, Trambly de Laissardière G, Pecheur P, Sadoc A and Dubois J M 1997 *J. Phys.: Condens. Matter* **9** 9585